

Coulomb repulsion versus Hubbard repulsion in a disordered chain

Franck Selva^a and Jean-Louis Pichard

CEA, Service de Physique de l'État Condensé, Centre d'Études de Saclay, 91191, Gif sur Yvette cedex, France

march 20, 2000

Abstract. We study the difference between on site Hubbard and long range Coulomb repulsions for two interacting particles in a disordered chain. While Hubbard repulsion can only yield weak critical chaos with intermediate spectral statistics, Coulomb repulsion can drive the two particle system to quantum chaos with Wigner-Dyson spectral statistics. For intermediate strengths U of the two repulsions in one dimension, there is a crossover regime where delocalization and spectral rigidity are maximum, whereas the limits of weak and strong U are characterized by a stronger localization and uncorrelated energy levels.

PACS. 05.45.+b Theory and models of chaotic systems – 73.10.-w Theories and models of many electron systems – 73.20.Jc Delocalization processes

1 Introduction

In low dimensions ($d \leq 2$) disorder always yields [1] a finite localization length L_1 when the particles do not interact and there is no spin-orbit scattering. When one wants to study the role of electron-electron interaction, a first issue is to know what kind of interaction is appropriate. When there are many carriers inside a large length L_1 (large density and weak disorder), it looks reasonable to assume weakly interacting Landau quasi-particles and to take the usual short range screened Coulomb repulsion. But, for low carrier densities (10^{10} - 10^{11} carriers per cm^2 is nowadays achieved [2] in two dimensional heterostructures) the screening of the charges is somewhat problematic and one may find safer to consider bare long range Coulomb repulsion. One has in this case a system having charge crystallization as a natural limit when kinetic energy becomes negligible compared to Coulomb energy. The range of the interaction can also be varied by metallic gates located in the vicinity of the electron gas, as it is often done for having a tunable carrier density. This gives us the motivation to study the difference between on site Hubbard-like repulsion and long range Coulomb repulsion in a simple limit: two electrons in a disordered chain. Since on-site interaction plays a role only if the orbital part of the wave function is symmetric, we restrict our study to the case with opposite spins.

The problem of two interacting particles (TIP) in one dimension has been mainly studied with on site Hubbard repulsion of strength U . As proposed by Shepelyansky [3] it has been numerically proven [4,5,6,7] that interaction delocalizes a certain number of TIP states over a length

$L_2 \gg L_1$. For a “contact” interaction as Hubbard repulsion, the TIP system exhibits remarkable properties [8,9,10,11]. The mixing of the one body states inside a scale $L = L_1$ and the associated delocalization effect for sizes $L \geq L_1$ is maximum for $U \approx U_c$, where U_c is the fixed point of a duality transformation [9] mapping the weak U/t limit onto the weak t/U limit, t being the kinetic energy scale. For the one body problem, the spectral statistics contains important information: an Anderson insulator has uncorrelated levels (Poisson statistics) whereas a disordered metal displays Wigner-Dyson rigidity characterizing quantum chaos. At the mobility edge, lies a scale invariant critical statistics [12], which exhibits a weaker spectral rigidity associated to weak critical chaos. For the TIP system with Hubbard interaction, the spectrum is Poissonian when $U \rightarrow 0$ and $U \rightarrow \infty$ and becomes [9] more rigid when $U \approx U_c$. However, the maximum possible rigidity does not correspond to Wigner-Dyson rigidity, but to an intermediate rigidity analogous to those characterizing the one body spectrum at a mobility edge (critical statistics). It was noticed in Ref. [10] that those intermediate statistics are also related to very slow interaction induced TIP diffusion at scales $L_1 \geq L \geq L_2$. We show in this study that, in contrast to Hubbard repulsion, Coulomb repulsion can drive the TIP one dimensional system to full quantum ergodicity with Wigner-Dyson statistics. From a statistical study of the interaction matrix elements coupling two free particle (2FP) states (i.e. the TIP eigenstates at $U = 0$), one finds that Coulomb repulsion mainly favors hopping terms between 2FP states nearby in energy, with energy separation of the order of the TIP level spacing $\Delta_2 \propto L^{-2}$. Hubbard repulsion mainly induces [9] hopping terms between 2FP states separated by a larger

^a e-mail: selva@drecam.saclay.cea.fr

energy $\Delta_2^{eff} > \Delta_2$, and the measure of the coupled 2FP states is multifractal [8]. However, the generic behavior of a TIP system with either Hubbard or Coulomb repulsions can be summarized by three regimes: a free particle limit dominated by Anderson localization; a large interaction limit dominated again by Anderson localization for Hubbard and by charge crystallization for Coulomb; and between those two Poissonian limits lies an intermediate regime characterized by a maximum mixing of the one particle states and a maximum delocalization effect. The intermediate regime in both cases is located around the interaction strengths U_c for which the TIP system has participation ratios of same order in both preferential eigenbases characterizing the weak and strong interaction limits.

2 TIP Hamiltonian

The TIP Hamiltonian \mathcal{H} is given by the sum of two terms: the first \mathcal{H}_t gives the kinetic energy (parameter t) and the random potentials (parameter W) in which the two particles can move,

$$\mathcal{H}_t = -t \sum_{\{i,j\}} c_i^+ c_j + W \sum_i v_i n_i. \quad (1)$$

v_i is randomly taken in the interval $[-\frac{1}{2}, \frac{1}{2}]$, c_i^+ creates a particle on the site i and $n_i = c_i^+ c_i$. The second term \mathcal{U} is the two body repulsion, which can be either on site Hubbard repulsion:

$$\mathcal{U} = U \sum_i n_i (n_i - 1) \quad (2)$$

or long range Coulomb repulsion:

$$\mathcal{U} = U \sum_i n_i (n_i - 1) + \frac{U}{2} \sum_{\substack{i,j=1 \\ |i-j| \leq L/2}}^L \frac{n_i n_j}{|i-j|} \quad (3)$$

The convention in this work is that two particles at the same site cost an energy $2U$ (and not U as assumed in previous refs. [8,9,10,11]). An additional cost of energy U/p has to be paid by two particles separated by a distance p with $L/2 \geq p \geq 1$ when there is Coulomb repulsion. The boundary conditions (BCs) are taken periodic.

Let us denote $(\epsilon_\alpha, \psi_\alpha)$ and $(E_{\alpha\beta}, \psi_{\alpha\beta})$ the eigenenergies and eigenfunctions of the one particle state $|\alpha\rangle$ and of the 2FP state $|\alpha\rangle \otimes |\beta\rangle = |\alpha\beta\rangle$ respectively. One has $E_{\alpha\beta} = \epsilon_\alpha + \epsilon_\beta$. The 2FP level spacing is $\Delta_2 \approx 2B/L(L+1)$ where the band width $B \approx 8t + 2W$. The one particle localization length L_1 is defined from the weak disorder formula $L_1 = 100/W^2$. Hereafter, the energies will be given in units of the kinetic energy hopping term t restricted to nearest neighbors.

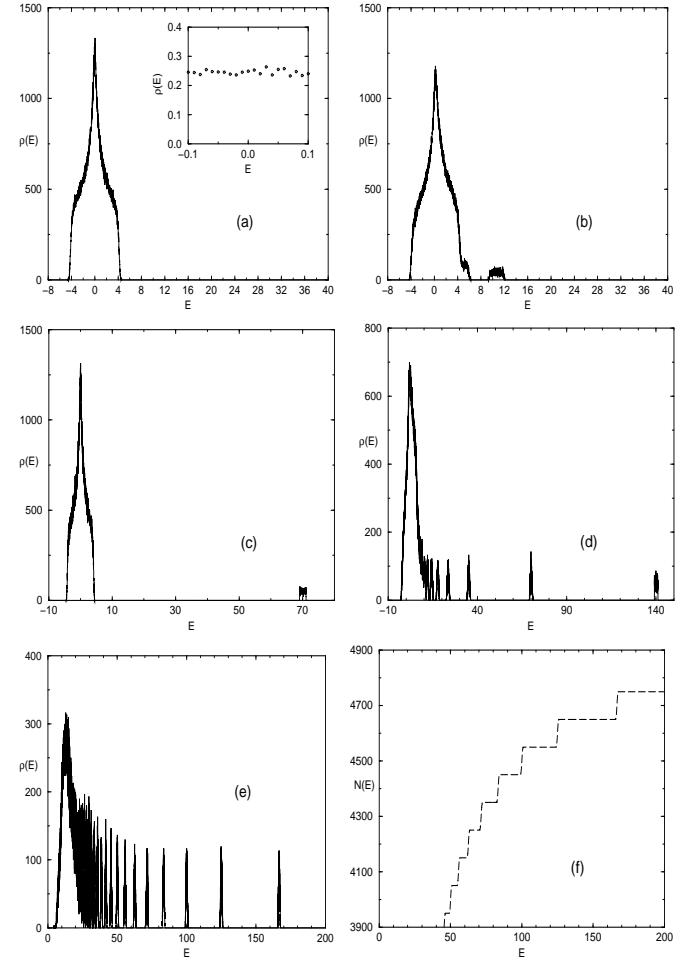


Fig. 1. Density of states $\rho_2(E)$ for $L = L_1 = 100$. (a) 2FP states ($U = 0$), insert: density around $E \approx 0$ (normalized to 1); (b) Coulomb ($U = 5$); (c) Hubbard ($U = 35$) The main band of $L(L-1)/2$ states remains centered around $E = 0$ together with L molecular states at $E \approx 2U$. Coulomb repulsion at (d) $U = 70$ and (e) $U = 500$. Each subband is centered at $E \approx U/d$ with $d = 0, \dots, L/2$. (f) Integrated density showing that each subband has L states for Coulomb repulsion ($U = 500$).

3 TIP density of states

When one compares the two repulsions, a first difference appears in the density of states $\rho_2(E)$. In the limit $U \rightarrow \infty$, Hubbard repulsion splits [9] the TIP band in two parts: a small band of L “molecular states” of high energy $\approx U + 2Wv_i$ corresponding to two electrons localized on the same site i and a main band of $L(L-1)/2$ “hard core boson” states which remain at the same small energies for $U \rightarrow \infty$ and $U \rightarrow 0$. The “hard core boson” states are given by the resymmetrization [13] of Slater determinants corresponding to electrons in the one body state $|\alpha\rangle$ and $|\beta\rangle$ respectively. Those states do not feel on site interaction, are not coupled to one another and become decoupled from the molecular states of much larger energies when $U \rightarrow \infty$. When one takes rigid BCs, the resymmetrization is simple and one has exactly $E_{\alpha\beta}(U \rightarrow 0) = E_{\alpha\beta}(U \rightarrow \infty)$ for $\alpha \neq \beta$. For two electrons in a ring enclosing a flux ϕ the resymmetrization is more

subtle and $E_{\alpha\beta}(\phi + \phi_0/2, U \rightarrow 0) = E_{\alpha\beta}(\phi, U \rightarrow \infty)$. For periodic BCs, $E_{\alpha\beta}$ ($\alpha \neq \beta$) goes to the corresponding 2FP eigenenergy with anti periodic BCs. In contrast to Hubbard repulsion where the majority of the TIP energy levels does not feel the interaction when $U \rightarrow \infty$, excepted L “molecular” states, Coulomb repulsion eventually crystallizes all the TIP states as two particle “molecules”. When L is even, the sizes of the molecules are $d = 0, \dots, L/2$ and the spectrum is split in $L/2$ subbands of L states ($d \neq L/2$) and one subband of $L/2$ states ($d = L/2$), each of them centered around an energy U/d . When N is odd, one has $(L+1)/2$ subbands of L states. Without disorder, each subband shrinks onto a single L -fold degenerate state obtained from successive translations of the “molecules” by one lattice spacing, a degeneracy which is broken by the random potentials. The different densities $\rho_2(E)$ induced by the two repulsions are illustrated in Fig. 1, for a chain of size $L = L_1 = 100$ and various interaction strengths U .

4 Crossover between two preferential eigenbases

When one turns on Hubbard repulsion, it has been detailed in Ref. [9] how the TIP system goes from the 2FP basis towards the “hard core boson basis” when $U \rightarrow \infty$. The interaction threshold $U_c = (24)^{1/4}t/2$ was defined (for energies near the band center) as the fixed point of the duality transformation mapping the distribution of the interaction matrix elements $\propto U/t$ which couple the 2FP states onto the distribution of the kinetic energy matrix elements $\propto t/U$ which couple the hard core boson states. At $U \approx U_c$, the 2FP basis ceases to be preferential compared to the hard core boson basis. Being unable to extend this duality argument for Coulomb interaction, we study the participation ratios PR_0 of the TIP wavefunctions $|\Psi\rangle$ onto the 2FP eigenbasis and PR_∞ onto the basis built out from symmetrized products of site orbitals (site basis). This later basis describes the correlated “molecules” created when $U \rightarrow \infty$.

$$PR_0 = \left(\sum_{\alpha\beta} |\langle \alpha\beta | \Psi \rangle|^4 \right)^{-1}$$

$$PR_\infty = \left(\sum_{ij} |\langle ij | \Psi \rangle|^4 \right)^{-1} \quad (4)$$

This allows us to extend for Coulomb repulsion the concept of a crossover threshold U_c where the $U = 0$ eigenbasis ceases to be preferential compared to the $U = \infty$ eigenbasis. As shown in Fig. 2, one has $U_c \approx 120$ when $L = L_1 = 50$ for Coulomb repulsion.

5 Interaction matrix elements in the 2FP basis

Before discussing the TIP spectral statistics, it is useful to study the structure of the interaction matrix elements

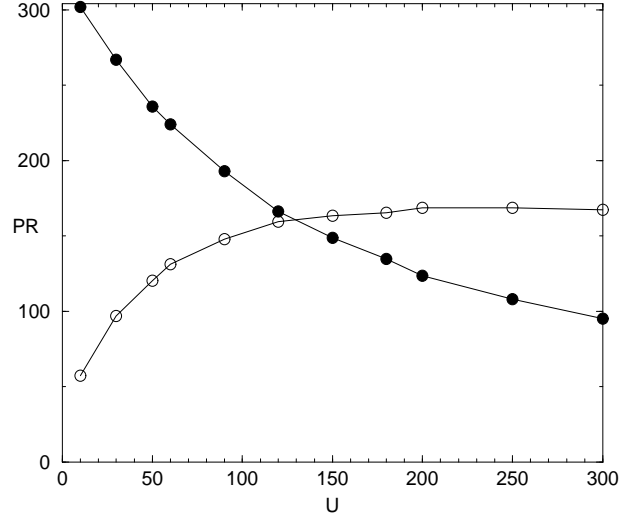


Fig. 2. Participation ratios PR_0 (○) and PR_∞ (●) of the TIP eigenstates of energies $\approx 2U/L$ onto the $U = 0$ and $U = \infty$ eigenbases respectively. $L = L_1 = 50$.

coupling the 2FP states. The 2FP wave function have components $\Psi_{\alpha,\beta}(n, m)$ on the sites $|nm\rangle$ given by

$$\langle \alpha\beta | nm \rangle = \frac{\psi_\alpha(n)\psi_\beta(m) + \psi_\alpha(m)\psi_\beta(n)}{\sqrt{2}}.$$

We denote

$$Q_{\alpha\beta}^{\gamma\delta}(0) = \sum_{n=1}^L \psi_\alpha^*(n)\psi_\beta^*(n)\psi_\gamma(n)\psi_\delta(n) \quad (5)$$

and

$$Q_{\alpha\beta}^{\gamma\delta}(p) = \sum_{n=1}^L \frac{\psi_\alpha^*(n)\psi_\beta^*(n+p)\psi_\gamma(n)\psi_\delta(n+p)}{|p|} + perm \quad (6)$$

where *perm* means the terms obtained after permuting $(\alpha \leftrightarrow \beta), (\gamma \leftrightarrow \delta)$, and $(\alpha \leftrightarrow \beta, \gamma \leftrightarrow \delta)$ for $p \neq 0$.

In the 2FP eigenbasis, the interaction matrix elements are

$$\langle \alpha\beta | \mathcal{U} | \gamma\delta \rangle = 4U Q_{\alpha\beta}^{\gamma\delta}(0) = U H_{\alpha\beta}^{\gamma\delta} \quad (7)$$

for Hubbard repulsion, and

$$\langle \alpha\beta | \mathcal{U} | \gamma\delta \rangle = U(4Q_{\alpha\beta}^{\gamma\delta}(0) + 2 \sum_{p=1}^{L/2} Q_{\alpha\beta}^{\gamma\delta}(p)) = UC_{\alpha\beta}^{\gamma\delta} \quad (8)$$

for Coulomb repulsion.

In the absence of disorder and with periodic BCs, the one body states are plane waves $\psi_\alpha(n) = (\exp ik_\alpha n)/\sqrt{L}$ and the interaction matrix elements $\mathcal{U}_{\alpha\beta}^{\gamma\delta}$ only couple 2FP states of same momentum $K = K_{\alpha\beta} = k_\alpha + k_\beta = K_{\gamma\delta}$. For Hubbard, one has when $L_1 \rightarrow \infty$

$$H_{\alpha\beta}^{\gamma\delta} \rightarrow \frac{4}{L} \delta_{K_{\alpha\beta}, K_{\gamma\delta}}. \quad (9)$$

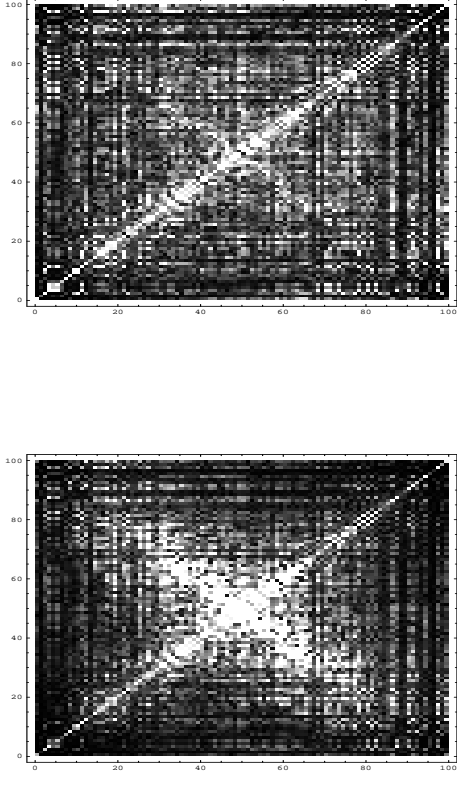


Fig. 3. Magnitude of the absolute value of the interaction matrix elements coupling a given state $|\alpha\alpha\rangle$ (with $\epsilon_\alpha \approx 0$) to L^2 states $|\gamma\delta\rangle$ for a typical sample with $L = 2L_1 = 100$. The L^2 absolute values are given in the plane (γ, δ) . The one particle states are ordered by increasing values of the energy. The white (black) points correspond to maxima (minima) with a linear scale of graduation. Top figure: Hubbard $H_{\alpha\alpha}^{\gamma\delta}$; Bottom figure: Coulomb $C_{\alpha\alpha}^{\gamma\delta}$

The interaction matrix has a block diagonal form. If L is odd, one has L blocks of size $N_s = (L+1)/2$. If N is even, one has $L/2$ blocks of size $N_s = L/2$ and $L/2$ other blocks of size $N_s = L/2 + 1$. The N_s TIP eigenenergies $E_n(K)$ of same momentum K are given by the N_s solutions of:

$$\sum_{\gamma\delta} \frac{1}{E_n(K) - E_{\gamma\delta}} = \frac{L}{4U} \quad (10)$$

where $E_{\gamma\delta} = 2 \cos k_\gamma + 2 \cos k_\delta$. The $E_n(K)$ alternate with the 2FP energies $E_{\gamma\delta}$ of same momentum. The TIP spectrum is the uncorrelated sum of L such series of different momenta K .

For Coulomb, the previous block diagonal structure is preserved when $L_1 \rightarrow \infty$, but each block becomes more

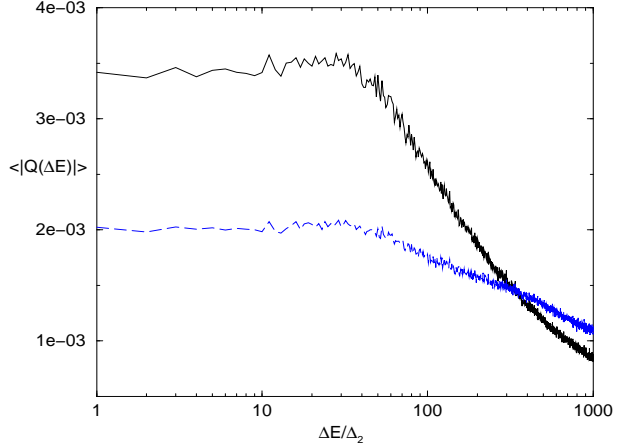


Fig. 4. Disorder average amplitudes $\langle |H_{\alpha\alpha}^{\gamma\delta}| \rangle$ (dashed line) and $\langle |C_{\alpha\alpha}^{\gamma\delta}| \rangle$ (continuous line) of the matrix elements coupling 2FP states separated by an energy $\Delta E = |E_{\alpha\alpha} - E_{\gamma\delta}|$ (in units of Δ_2) for $L = 2L_1 = 100$.

complex:

$$\begin{aligned} C_{\alpha\beta}^{\gamma\delta} \rightarrow & \frac{4}{L} \delta_{K_{\alpha\beta}, K_{\gamma\delta}} \times & (11) \\ & \left(1 + \sum_{p=1}^{L/2} \frac{\exp -i[(k_\beta - k_\gamma)p]}{2p} + \sum_{p=1}^{L/2} \frac{\exp -i[(k_\beta - k_\delta)p]}{2p} \right. \\ & \left. + \sum_{p=1}^{L/2} \frac{\exp -i[(k_\alpha - k_\gamma)p]}{2p} + \sum_{p=1}^{L/2} \frac{\exp -i[(k_\alpha - k_\delta)p]}{2p} \right) \end{aligned}$$

In the presence of a random potential, the absolute values of the matrix elements can be given using a linearly graduated grey scale in the plane (γ, δ) for a given 2FP state $|\alpha\beta\rangle$, the one body states $|\gamma\rangle$ and $|\delta\rangle$ being ordered by increasing energies. When W is sufficiently small, TIP momentum remains almost conserved and one can see in the plane (γ, δ) a white cross made by the two diagonals if $\alpha = \beta$. The first diagonal corresponds to coupling to other states $|\gamma\delta\rangle$ with $|\gamma| \approx |\delta|$, the second to coupling to 2FP states $|\gamma\delta\rangle$ close in energy ($E_{\alpha\beta} \approx E_{\gamma\delta}$). When W is larger, Coulomb and Hubbard give rise to a different pattern in the (γ, δ) plane: energy-momentum conservation remains partially preserved by Coulomb repulsion (the second diagonal persists) and is lost by Hubbard repulsion, as shown in Fig. 3 for $L \approx 2L_1 = 100$. 2FP states $|\alpha\alpha\rangle$ with $\epsilon_\alpha \approx 0$ are considered in Fig. 3, but similar conclusions can be drawn from arbitrary 2FP states $|\alpha\beta\rangle$.

To explain why $C_{\alpha\beta}^{\gamma\delta}$ continues to mainly couple $|\alpha\beta\rangle$ to states $|\gamma\delta\rangle$ nearby in energy, we note that when L_1 is finite, disorder smears the sharp delta function into a broader gaussian peak of width $\sigma \propto L_1^{-1}$. $\langle \delta_{K_{\alpha\beta}, K_{\gamma\delta}} \rangle \rightarrow \exp -(K_{\alpha\beta} - K_{\gamma\delta})^2 / (2\sigma^2)$ and $\langle \exp -i(k_\alpha - k_\beta)p \rangle \rightarrow \exp -(k_\alpha - k_\beta)^2 / (2\sigma^2)$, one gets respectively

$$H_{\alpha\beta}^{\gamma\delta} \propto \exp -\frac{(K_{\alpha\beta} - K_{\gamma\delta})^2}{2\sigma^2}$$

and

$$C_{\alpha\beta}^{\gamma\delta} \propto \exp\left(-\frac{(K_{\alpha\beta} - K_{\gamma\delta})^2}{2\sigma^2}\right) \times \left[2 - \ln\left(\frac{|k_\beta - k_\gamma|}{\sigma}\right) - \ln\left(\frac{|k_\beta - k_\delta|}{\sigma}\right) - \ln\left(\frac{|k_\alpha - k_\gamma|}{\sigma}\right) - \ln\left(\frac{|k_\alpha - k_\delta|}{\sigma}\right)\right] \quad (12)$$

This explains the behavior shown in Fig. 4 where the disorder averaged amplitude of the hopping terms are given as a function of the energy difference. The L hopping terms between the 2FP states $|\gamma\delta\rangle$ nearby in energy ($\Delta E \leq \Delta_2 L/2$) are much smaller for Hubbard than for Coulomb. For larger energy separation ΔE , there is a $\ln(|\Delta E/\Delta_2|)$ decay which is more pronounced for Coulomb than for Hubbard.

6 TIP diffusion and 2FP lifetime

Coulomb repulsion couples a density $\approx \rho_2$ of 2FP states nearby in energy. Hubbard repulsion effectively couples a smaller density $\rho_2^{eff} < \rho_2$, as explained in Ref. [8]. Let us review three consequences of this difference.

(i) TIP diffusion: In the first studies [3,14,15] of the TIP problem, a density $\rho_2(L_1)$ of 2FP states coupled by the interaction was assumed for $L \approx L_1$. Under this assumption, it was predicted that the TIP dynamics should exhibit interaction assisted diffusion on scales $L_1 < L < L_2$, the time evolution of the TIP center of mass R_2 being given [15] by:

$$R_2(t) \approx \sqrt{D_2(t)t} \quad (13)$$

with $D_2(t)$ is roughly constant, up to $\log(t)$ corrections [15]. In Ref. [10], a much slower propagation $R_2 \propto \log t$ was observed for Hubbard repulsion, attributed to the weak density $\rho_2^{eff}(L_1)$ of effectively coupled states. One expects that the original prediction will be at least partially restored for Coulomb repulsion.

(ii) TIP localization: The interaction assisted propagation stops at a scale L_2 characteristic of TIP localization. Assuming $|<\alpha\beta|\mathcal{U}|\gamma\delta>|^2 \propto U^2/L_1^3$ for $L \approx L_1$, the enhancement factor L_2/L_1 was originally given by the estimate:

$$\frac{L_2}{L_1} \propto |<\alpha\beta|\mathcal{U}|\gamma\delta>|^2 \rho_2(L_1) \propto L_1 \quad (14)$$

It was pointed out in Ref. [8] that, since $\rho_2(L_1) \propto L_1^2 \rightarrow \rho_2^{eff}(L_1) \propto L_1^{1.75}$ in the presence of Hubbard repulsion, the enhancement factor should be weaker ($L_2/L_1 \propto \sqrt{L_1}$), a prediction confirmed by numerical calculations. It is likely that $L_2/L_1 \propto L_1$ will be a better estimate for Coulomb repulsion.

(iii) 2FP lifetime: The inverse lifetime ($\Gamma_{\alpha\beta}$) of a 2FP state $|\alpha\beta\rangle$ is given by Fermi Golden rule:

$$\Gamma_{\alpha\beta} \propto \sum_{\gamma\delta} |<\alpha\beta|\mathcal{U}|\gamma\delta>|^2 \delta(E_{\alpha\beta} - E_{\gamma\delta}) \quad (15)$$

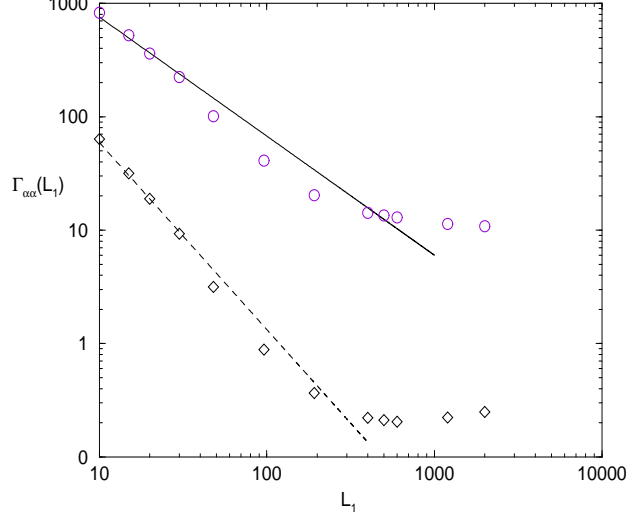


Fig. 5. Inverse lifetime $\Gamma_{\alpha\alpha}(L_1)$ of a 2FP state $|\alpha\alpha\rangle$ with $\epsilon_\alpha \approx 0$ for Hubbard (\diamond) and Coulomb (\circ) repulsion respectively. $L = 420$. The continuous (dashed) line corresponds to $\Gamma_{\alpha\alpha} \propto L_1^{-1.65}$ ($\propto L_1^{-1.05}$).

If the density of coupled states is $\rho_2(L_1) \approx L_1^2$, a reasonable estimate for Coulomb repulsion, one gets

$$\Gamma_{\alpha\beta}(L = L_1) \propto |<\alpha\beta|\mathcal{U}|\gamma\delta>|^2 \rho_2(L_1) \propto L_1^{-1}.$$

In contrast, the lifetime should be longer for Hubbard repulsion:

$$\Gamma_{\alpha\beta}(L = L_1) \propto |<\alpha\beta|\mathcal{U}|\gamma\delta>|^2 \rho_2^{eff}(L_1) \propto L_1^{-1.65}$$

since the density [8] of coupled states (by the second moment of $|<\alpha\beta|\mathcal{U}|\gamma\delta>|$) is $\rho_2^{eff} \propto L_1^{1.35}$ for a 2FP state $|\alpha\alpha\rangle$.

We have checked this prediction. In Fig. 5, the inverse lifetime calculated in a chain of length $L = 420$ is shown as a function of L_1 . When $L_1 < L$, one has $\Gamma_{\alpha\alpha} \propto L_1^{-1.65}$ for Hubbard repulsion while $\Gamma_{\alpha\alpha} \propto L_1^{-1.05}$ for Coulomb repulsion, close to a simple decay $\propto L_1^{-1}$. When L becomes larger than L_1 , the lifetime becomes L -independent for Hubbard, and may continue to weakly decay as a function of L for Coulomb. Fig. 5 shows us that this possible decay remains negligible.

7 Two particle spectral statistics

We now study how the spectral statistics depend on the interaction strength U for the two repulsions, using the distribution $P(s)$ of energy spacings between consecutive levels and the variance $\Sigma_2(E)$ of the number of levels inside an energy window of width E . We consider energy levels in the bulk of the low energy sub-band: $E \approx 0$ for Hubbard repulsion and $E \approx 2U/L$ for Coulomb repulsion (see Fig. 1). We take $L = L_1$ for having the largest interaction matrix elements, and hence the maximum mixing of the 2FP states.

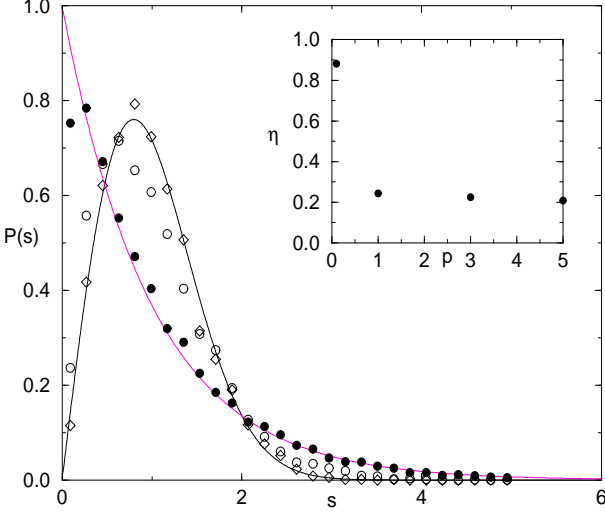


Fig. 6. Spacing distribution $P(s)$ for Hubbard (●) and Coulomb (◊) repulsions at $U = 70$ and $L = L_1 = 50$. The symbols (○) correspond to a medium range interaction truncated to $p = 1$. The levels are taken around $E \approx 2U/L$ for Coulomb repulsion and around $E \approx 0$ otherwise. The continuous lines correspond to $P_P(s)$ and $P_W(s)$ respectively. Insert: Parameter η around $E \approx 0$ as a function of the range p of the interaction.

After unfolding the spectra, one expects

$$P(s) \approx P_W(s) \approx \frac{\pi s}{2} \exp\left(-\frac{\pi}{4}s^2\right) \quad (16)$$

and

$$\Sigma_2(E) \approx \Sigma_2^W(E) \approx \frac{2}{\pi^2} \left(\ln(2\pi E) + \gamma + 1 - \frac{\pi^2}{8} \right) \quad (17)$$

(γ being the Euler constant) for correlated levels having Wigner-Dyson statistics, whereas one should have Poisson statistics with

$$P_P(s) = \exp(-s) \quad (18)$$

and

$$\Sigma_2^P(E) = E \quad (19)$$

for uncorrelated levels.

The TIP spectra are well described by Wigner-Dyson statistics for an intermediate Coulomb repulsion. In Fig. 6 and in Fig. 7, one can see indeed that the level spacing distribution and the number variance Σ_2 are well described by the Wigner surmise $P_W(s)$ and $\Sigma_2^W(E)$ respectively near the intermediate interaction strength $U_c \approx 120$ for which the TIP system does not have a preferential eigenbasis (see Fig. 2). As shown by $\Sigma_2(E)$ (Fig. 7), Wigner-Dyson spectral rigidity is established over an energy interval containing a few levels. In contrast, Hubbard repulsion can only yield [9] at the corresponding U_c (≈ 1)

$$P_{SP} \approx 4s \exp(-2s) \quad (20)$$

and

$$\Sigma_2 \approx 0.16 + 0.41E \quad (21)$$

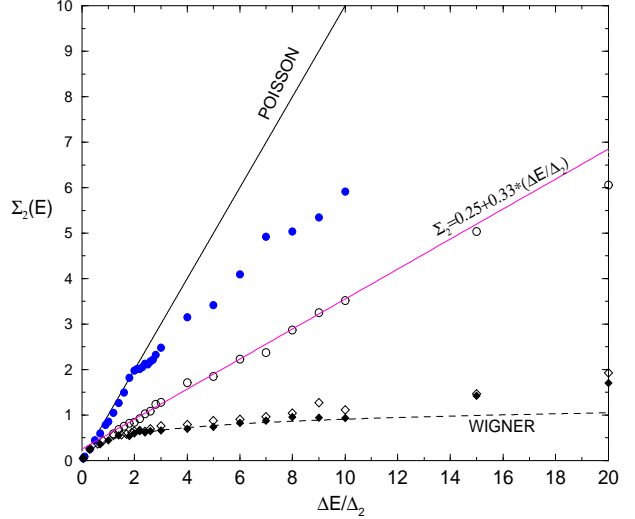


Fig. 7. Number variance Σ_2 as a function of the energy interval E in units of TIP level spacing Δ_2 (same symbols as in Fig. 6 excepted the filled diamonds (Coulomb at $U = 100$ and $L = L_1 = 100$)).

respectively.

To study how the spacing distribution depends on U , we use the spectral parameter η defined by

$$\eta(P, U) = \frac{\int_0^b ds [P(s) - P_W(s)]}{\int_0^b ds [P_P(s) - P_W(s)]} \quad (22)$$

with $b = 0.4729$. For $U = 0$, the consecutive levels are essentially uncorrelated and $\eta \approx 1$. The curves $\eta(U)$ given in Fig. 9 show us a striking difference between the spectral statistics yielded by the two repulsions.

For $L = L_1 = 100$, let us estimate the interaction threshold U^* for which the interaction matrix elements coupling consecutive 2FP states becomes of the order of their energy separation Δ_2 . $\rho_2 \approx 0.25$ (density normalized to 1) gives $\Delta_2 \approx (\rho_2 L(L+1)/2)^{-1} \approx 4/5050$ (see insert of Fig. 1) for the energy spacing between consecutive 2FP levels around $E = 0$. The off-diagonal interaction matrix elements $Q = H_{\alpha\beta}^{\gamma\delta}$ (Hubbard) or $Q = C_{\alpha\beta}^{\gamma\delta}$ (Coulomb) coupling consecutive 2FP levels are normally distributed, as shown in Fig. 8. The root mean square of Q is small for Hubbard (≈ 0.0038) and larger for Coulomb (≈ 0.01). This gives $U_C^* \approx 0.08$ for Coulomb and $U_H^* \approx 0.2$ for Hubbard.

When U increases but remains lower than U^* , there is first a perturbative regime discussed in Refs. [16,17] where the interaction yields Rabi oscillations between consecutive 2FP states at a frequency given by the absolute value of the coupling interaction matrix element. Moreover, the energy range E_U under which one has level repulsion is given [16] by this Rabi frequency. When U becomes equal to U^* , one has a transition from this perturbative regime towards an effective Fermi golden rule decay of the 2FP states and the characteristic range E_U over which Wigner-Dyson rigidity occurs becomes [16,17] proportional to the square of the amplitude of the coupling

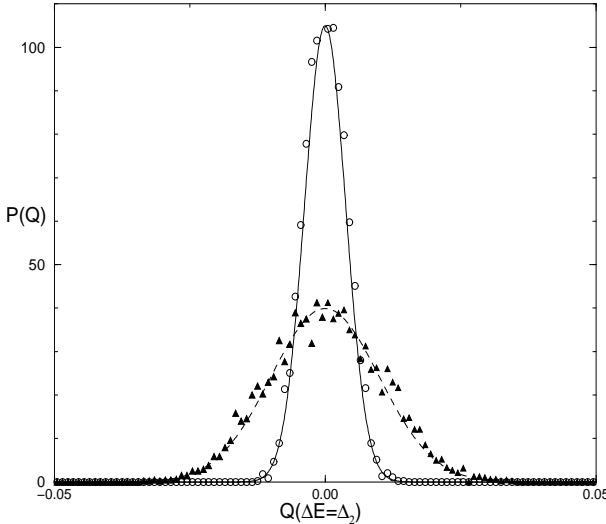


Fig. 8. Distribution $P(Q)$ of the interaction matrix elements $Q = H_{\alpha\beta}^{\gamma\delta}$ (Hubbard: circle) or $Q = C_{\alpha\beta}^{\gamma\delta}$ (Coulomb: triangle) coupling nearest neighbor 2FP states (energy separation $\approx \Delta_2$) for $L = L_1$. The distributions are fitted with gaussian curves of variance $\sigma^2 = 0.01^2$ (Coulomb, dashed line) and $\sigma^2 = 0.0038^2$ (Hubbard, continuous line).

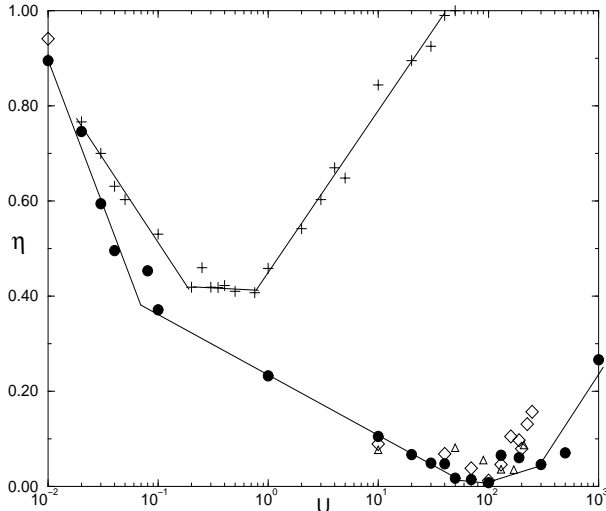


Fig. 9. Spectral parameter η as a function of U for $L = L_1$. Levels around $E \approx 2U/L$ for Coulomb repulsion with $L = 100(\bullet)$, $50(\diamond)$ and $65(\triangle)$. Levels around $E \approx 0$ for Hubbard repulsion (+) with $L = 100$.

matrix elements: $E_U \propto U$ when $U < U^*$ and $E_U \propto U^2$ when $U > U^*$. $U = U^*$ is the interaction threshold where the spectral statistics are intermediate between Poisson and Wigner ($\eta \approx 0.39$ when $P(s) \approx P_{SP}(s)$). Looking at Fig. 9, one can see that η decreases as a function of U down to the characteristic value $\eta^* \approx 0.39$ reached when $U \approx U_C^* \approx 0.08$ for Coulomb repulsion, and when $U \approx U_H^* \approx 0.2$ for Hubbard repulsion.

For Coulomb repulsion, η continues to decrease when $U \geq U_C^*$ down to $\eta = 0$ with the slower U dependence characteristic of the effective golden rule decay of the 2FP

states. The Wigner-Dyson distribution $P_W(s)$ is fully established at $U \approx U_c$, i.e. when the TIP system is exactly as far from the $U = 0$ eigenbasis than from the $U = \infty$ eigenbasis. When $U \geq U_c$, integrability is slowly restored and $\eta \rightarrow 1$ as $U \rightarrow \infty$.

For Hubbard repulsion, the spectral rigidity does not continue to increase above U_H^* , but saturates to the intermediate critical rigidity characterized by Eq. 20 and Eq. 21 for $P(s)$ and $\Sigma_2(E)$ respectively. Above the fixed point $U_c \approx 1$ of the duality transformation, the TIP system becomes closer to the $U = \infty$ eigenbasis and the levels become statistically uncorrelated. This critical Hubbard regime is a complicated issue where the multifractal character of the interaction matrix described in ref. [8] is very likely relevant. However, one can do the following remark. When $L_1 \rightarrow \infty$, the interaction matrix is block diagonal, a block corresponding to a pair momentum K . For Hubbard, the N_s TIP level $E_n(K)$ of momentum K are located near the 2FP levels of same momentum when $4U/L \rightarrow 0$ or $4U/L \rightarrow \infty$. One can assume that they should be near the middle of consecutive 2FP levels of same K for $U \approx U_c$. The distribution $P(s)$ of levels located in the middle of levels with spacing distribution $P_P(s)$ is the semi-Poisson distribution $P_{SP}(s)$. If the sequence of 2FP levels of momentum K were randomly distributed, the spacing distribution of the N_s TIP levels should be given by $P_{SP}(s)$ without disorder. On the contrary, the interaction matrix being more random for Coulomb, one can expect that the L series of N_s levels of momentum K will be driven towards Wigner-Dyson statistics as U increases. However, though the argument may give hints for the existence of the Hubbard $P_{SP}(S)$, it does not explain the behavior of $\Sigma_2(E)$. The breakdown of momentum conservation by the disorder, and the associated mixing of the L independent series of N_s levels characterizing the clean limit plays a complex role.

The insert of Fig. 6 shows how the spectrum becomes more rigid at $U = 70$ when the range p of the interaction is increased. $\Sigma_2(E)$ displays a similar information in Fig. 7.

8 Quantum melting for intermediate Coulomb repulsions

The intermediate Wigner-Dyson regime yielded by Coulomb repulsion corresponds, inside a scale L_1 , to a complete melting of the localized 2FP states previous to crystallization. To show this, we introduce two parameters γ and ξ . For a TIP wavefunction $|\Psi\rangle$, we calculate the density $\rho_i = \langle \Psi | c_i^\dagger c_i | \Psi \rangle$ at site i and the density density correlation function $C(r) = (1/2) \sum_i \rho_i \rho_{i-r}$. The participation ratio ξ (i.e. the number of sites occupied by a TIP state) is given by $2C(0)^{-1}$. The crystallization parameter γ is given by the difference $\text{Max}C(r) - \text{Min}C(r)$, where all translations r (including $r = 0$) are considered. If the electron density is homogeneous (as for an extended liquid state) $\gamma \approx 0$ whereas $\gamma \approx 1$ if the two charges are mainly located on two different sites, a situation occurring when $U \rightarrow \infty$.

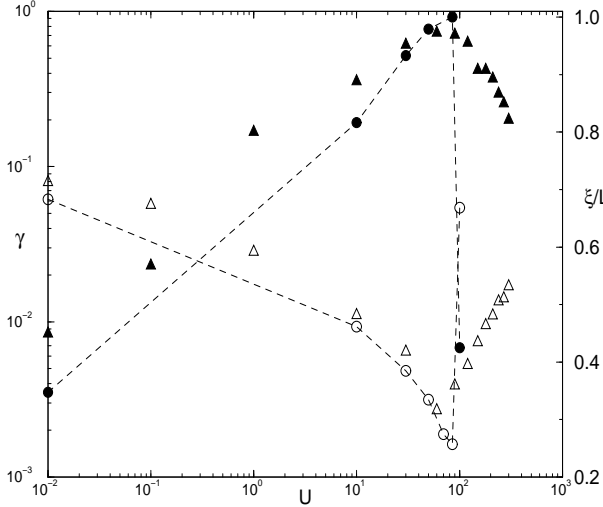


Fig. 10. Crystallization parameter γ for $L = L_1 = 50(\Delta)$ and $100(\circ)$ and the corresponding numbers of occupied sites ξ (filled symbols) for Coulomb repulsion for TIP levels around $E = 2U/L$.

(Coulomb “molecule”) and when $U \rightarrow 0$ and $L_1 \rightarrow 0$ (two electrons located in two minima of the potential). The variations of ξ and γ are given in Fig. 10 when Coulomb repulsion U increases. The curves $\gamma(U)$ and $\xi(U)$ are correlated to the curve $\eta(U)$ shown in Fig. 9. The curve $\xi(U)$ shows us that the TIP states occupy a fraction of the chain without repulsion before being uniformly spread over a scale L_1 at interaction strength $U \approx U_c$ for which there is a crossing of the two curves $PR(U)$ given in Fig. 2. For $L = L_1$, one has an interaction induced quantum melting of the non interacting glass, yielding quantum ergodicity with “more liquid” and extended wavefunctions and Wigner-Dyson spectral statistics.

9 Conclusions

We have studied one of the simplest problems where quantum localization and two body interaction are in competition. We have seen that the range of the interaction makes important differences. One of them is revealed by the study of the spectral statistics, providing an intriguing puzzle for quantum ergodicity: the Wigner-Dyson statistics shrinking to intermediate statistics when the two body repulsion becomes local. However, the generic behavior of the TIP system can be summarized by three regimes, independently of the interaction range. There is the free particle limit dominated by quantum localization, the Coulomb limit dominated by the pinning of a correlated system of charges (“Coulomb molecule, Wigner crystal”) or by quantum localization again (Hubbard repulsion). Between these two limits, there is an intermediate regime where one has a maximum mixing of the one body states, making the states more extended and the spectrum more rigid. In one dimension, this yields a partial delocalization effect (L_2 could be large but remains finite). Similar conclusions have been reached from a study of the many body ground state

[18] of one dimensional spinless fermions at half filling. In two dimensions, there are experimental evidences [2] that localization may disappear for intermediate Coulomb energy to Fermi energy ratios r_s . A new quantum regime has been observed [19] for the ground state of two dimensional spinless fermions at intermediate factors r_s where the metallic phase is observed. The nature of the states, when the system is far from the free particle (Fermi glass) or the Coulomb (Wigner crystal) bases, and the associated transport mechanism, remain to be understood. This simple one dimensional study draws our attention to the important role played by the range of electron-electron repulsions. To know how is or is not screened Coulomb repulsion in low density electron systems is then an important issue.

References

1. E. Abrahams, P.W. Anderson, D.C. Licciardello and T.V. Ramakrishnan, Phys. Rev. Lett. **42**, 693 (1979).
2. S. V. Kravchenko et al, Phys. Rev. B **50**, 8039 (1995); J. Yoon et al, Phys. Rev. Lett. **82**, 1744 (1999); M. Y. Simmons et al, Phys. Rev. Lett. **80**, 1292 (1999).
3. D. L. Shepelyansky, Phys. Rev. Lett. **73**, 2067 (1994).
4. See Chapter 4 in “Correlated Fermions and Transport in Mesoscopic Systems”, T. Martin, G. Montambaux and J. Trần Thanh Vân editors, Editions Frontières (1996).
5. D. Weinmann, A. Müller-Groeling, J.-L. Pichard and K. Frahm, Phys. Rev. Lett. **75**, 1598 (1995).
6. F. Von Oppen et al., Phys. Rev. Lett. **76**, 491 (1996).
7. K. Frahm, Eur. Phys. J. B **10**, 371 (1998).
8. X. Waintal and J.-L. Pichard, Eur. Phys. J. B **6**, 117 (1998).
9. X. Waintal, D. Weinmann and J.-L. Pichard, Eur. Phys. J. B **7**, 451 (1999).
10. S. De Toro Arias, X. Waintal and J.-L. Pichard, Eur. Phys. J. B **10**, 149 (1999).
11. A. Wobst and D. Weinmann, Eur. Phys. J. B **10**, 159 (1999).
12. B. I. Shklovskii et al, Phys. Rev. B **47**, 11487 (1993).
13. I. V. Ponomarev and P. G. Silvestrov, Phys. Rev. B **56**, 3742 (1997).
14. Y. Imry, EuroPhys. Lett. **30**, 405 (1995).
15. K. Frahm, A. Müller-Groeling and J.-L. Pichard, Phys. Rev. Lett. **76**, 1509 (1996).
16. D. Weinmann and J.-L. Pichard, Phys. Rev. Lett. **77**, 1556 (1996).
17. D. Weinmann, J.-L. Pichard and Y. Imry, J. Phys. I France **7**, 1559 (1997).
18. P. Schmitteckert, R. Jalabert, D. Weinmann and J.-L. Pichard, Phys. Rev. Lett. **81**, 2308 (1998).
19. G. Benenti, X. Waintal and J.-L. Pichard, Phys. Rev. Lett. **83**, 1826 (1999).